LWT - Food Science and Technology 90 (2018) 346–353

Contents lists available at ScienceDirect

LWT - Food Science and Technology

journal homepage: www.elsevier.com/locate/lwt

Growth and characterization of spherical cinnamon nanoparticles: Evaluation of antibacterial efficacy

Ali Aqeel Salim[a], Noriah Bidin[a,*], Sib Krishna Ghoshal[b]

[a] Laser Center, Institute for Scientific and Industrial Research, Universiti Teknologi Malaysia, 81300, Johor Bahru, Skudai, Malaysia
[b] Advanced Optical Materials Research Group, Physics Department, Faculty of Science, Universiti Teknologi Malaysia, 81300, Johor Bahru, Skudai, Malaysia

ARTICLE INFO

Keywords:
CNPs
Laser ablation
Optical properties
Morphology
Antibacterial drugs

ABSTRACT

Organic nanoparticles with controlled properties are advantageous for diversified biomedical and pharmacological applications. Cinnamon nanoparticles (CNPs) being bioactive and nontoxic can be effective antibacterial agents. Driven by this idea, we prepared spherical CNPs using pulse laser ablation in liquid (PLAL) technique and characterized these NPs. A pure cinnamon target immersed in liquid ethanol (5 mL) was ablated using Q-switched Nd:YAG pulse laser of varying energy (30–180 mJ). Laser energy dependent structure, morphology and optical properties of the as-grown CNPs were determined. Furthermore, the antibacterial activity of such CNPs against four bacterial strains (*Escherichia coli, Staphylococcus aureus, Bacillus subtilis* and *Pseudomonas aeruginosa*) was evaluated using agar well diffusion and optical density measurements. These CNPs were demonstrated to be beneficial for the development of antibacterial drugs and food processing.

1. Introduction

Organic compounds, with particle size above 100 nm, can be converted by mechanical milling methods. However, these approaches are limited as numerous applications demand particles tinier than 100 nm (An, Kwon, Jung, & Park, 2002; Müller, Jacobs, & Kayser, 2001). Particles of nanometric dimension can be achieved using re-precipitation of organic molecules, where such organic solution can rapidly be injected into a poor solvent with/without a surfactant to form molecular precipitates (An et al., 2002). Formerly, several techniques were used to synthesize various organic NPs including pulse laser ablation in liquid (PLAL), chemical etching, ball milling, sol-gel, molecular condensation, microorganism, etc. Each of these methods has its own advantage to produce NPs with controlled morphology and composition dependent properties (Asahi, Sugiyama, & Masuhara, 2008; Salim & Bidin, 2017). Compared to nanoemulsion (Yildirim, Oztop, & Soyer, 2017; Zhang, Zhang, Fang, & Liu, 2017) and chemical (Ganeev, Baba, Ryasnyansky, Suzuki, & Kuroda, 2004) techniques, PLAL technique is very useful due to its ease, economic, eco-friendly and large-scale reproducibility of contaminant free nanostructures (Sajti, Sattari, Chichkov, & Barcikowski, 2010; Sylvestre, Kabashin, Sacher, Meunier, & Luong, 2004). Moreover, the nature of the nanostructures obtained via PLAL technique is decided by the laser characteristics such as the lasing wavelength, the pulse width, the repetition rate, the fluence and the exposure time (Zhang, Gökce, & Barcikowski, 2017; Sylvestre et al., 2004; Tsuji, Iryo, Nishimura, & Tsuji, 2001).

Research revealed that increase in the laser power can improve the nanoparticles productivity (Wagener, Schwenke, Chichkov, & Barcikowski, 2010). It is established that the laser parameters play a significant role in controlling the nanoparticles morphology by delivering favourable thermodynamic conditions during the growth process (Zhang, Gökce, et al., 2017). In the ablation process, the laser interacts with the material (target) and creates hot and dense plasma on the target surface, wherein an expanding bubble is formed during the optical inactivation period of the plasma (Tsuji et al., 2001). Subsequently, NPs are released in the liquid environment after the bubble is collapsed (Wagener et al., 2010). It is found that the lifetime of the cavitation bubble become longer with the increase of the laser fluence and the repetition rate, which in turn increase the productivity of NPs.

Currently, products from different parts of the aromatic plants have been extensively used for biomedicinal purposes (Ahmad et al., 2010; Jeyaratnam et al., 2016). Compared to metallic nanomaterials, the organic nanoparticles produce from natural herbs are favored due to the presence of rich of active agents, biocompatibility, abundance, easy stabilization and safe handling (Gopinath et al., 2012; Yang et al., 2010). Polyphenol and cinnamaldehyde compounds in cinnamon cassia have been used worldwide as traditional herbal medicine and healthy nutrition element. Unique attributes including safe, bioactivity, non-toxicity and anti-bacterial efficacy make cinnamon compounds suitable for different applications (Chang, Chen, & Chang, 2001; Fatima, Zaidi,

* Corresponding author.
E-mail addresses: asali8@live.utm.my (A.A. Salim), noriah@utm.my (N. Bidin), sibkrishna@utm.my (S.K. Ghoshal).

https://doi.org/10.1016/j.lwt.2017.12.047
Received 20 September 2017; Received in revised form 14 December 2017; Accepted 19 December 2017
Available online 21 December 2017
0023-6438/

Amraiz, & Afzal, 2016). Yet, the bioactivity of cinnamon components (liquid or powder) against bacterial cell has not been well understood (Sathishkumar et al., 2009). In-depth understanding of the antibacterial effectiveness may require an accurate synthesis method to produce CNPs with controlled morphology. Subsequent implementation of such CNPs in the bacterial cell is needed to examine their cell wall penetrability and concomitant destruction of DNA (Basniwal, Buttar, Jain, & Jain, 2011).

Earlier, metal nanoparticles using cinnamon as a stabilizing agent for biomedical applications (especially as antibacterial agent) have been widely investigated (Huang et al., 2007; Ma, Davidson, Critzer, & Zhong, 2016; Salim, Bidin, Lafi, & Huyop, 2017; Sathishkumar et al., 2009). Cinnamon leaf with aqueous Au and Ag precursors at ambient temperature has also been synthesized for anticancer drug development (Huang et al., 2007). The presence of polyphenols components in cinnamon was considered to be beneficial for the reduction of Ag and Au ions (Huang et al., 2007). According to Ma et al. (Ma et al., 2016), the ethylenediaminetetraacetate can overcome the antagonistic effect of the lauric arginate and the cinnamon oil combination against Gram-negative bacteria. Using nanoemulsions technique, Zhang et al. (Zhang, Zhang, et al., 2017) investigated the bioactivity of cinnamon oil against some pathogenic microorganisms. The morphological properties of diverse cinnamon nanostructures produced inside different growth media including citric acid, ethanol, methanol and olive oil (Salim & Bidin, 2017; Salim et al., 2017) have been widely studied. So far, an accurate preparation method for CNPs with desired morphology and antibacterial activities is far from being achieved. On top, the structural and antibacterial properties of CNPs produced in ethanol media have never been evaluated. Thus, the main purpose of this paper is to produce better CNPs morphologies inside ethanol as growth media using PLAL technique for examining the feasibility of achieving their enhanced antibacterial effectiveness.

This paper reports the eco-friendly synthesis of CNPs (grown inside ethanol medium) using inexpensive PLAL technique. The influence of changing laser ablation energy (30–180 mJ) on the growth mechanism of CNPs was inspected. As-prepared CNPs were characterized using various analytical tools. Furthermore, the antibacterial efficiency of these CNPs was evaluated on Gram-negative and Gram positive bacterial strains. Agar well diffusion assay and optical density (OD_{600}) measurements were performed to determine the antibacterial effectiveness.

2. Experimental

2.1. Materials used

Cinnamon cassia sticks were purchased from the local supermarket (Aeon, Malaysia). Analytical grade ethanol (C_2H_5OH, 96% purity) was purchased from Sigma Aldrich (utilized as liquid media). Broth media (Merck, Sigma Aldrich) including Nutrient Agar and Mueller Hinton Agar were used for all the bacterial cultures. Penicillin-streptomycin (Sigma Aldrich) was applied for evaluating the antibacterial activity of CNPs. Furthermore, two representative microorganisms of Gram (negative and positive) bacteria strain *Bacillus subtilis* (BS) ATCC 21332, *Pseudomonas aeruginosa* (PA) ATCC 27853, *Staphylococcus aureus* (SA) ATCC 11775 and *Escherichia coli* (EC) ATCC 25923 were acquired from the Microbiology Research Laboratory, Universiti Teknologi Malaysia. Each cinnamon stick was cut into a dimension of (20 mm × 10 mm × 2 mm) and washed using analytical grade (acetone) in an ultrasonic bath for 60 min. Then, these sticks were rinsed using distilled water to remove the organic contaminants.

2.2. Cinnamon nanoparticles synthesis

The PLAL technique (Fig. 1) was used to prepare the CNPs, wherein a Q-switched 1064-Nd: YAG laser of 10 ns pulse duration, 1 Hz repetition rate, and under varying ablation energy (in the range of 30–180 mJ with spot size of 2 mm) was used to irradiate the cinnamon target. The stick was immersed at the bottom of cubic pyrex container of dimension (3 cm × 3 cm × 3 cm) filled with 5 mL of liquid ethanol as growth medium (at room temperature). The laser beam was focused onto the surface of the target at the laser repetition rate of 1000 pulse/sec. To achieve the optimum growth, the separation between the lens and the surface target was kept fixed (17 mm) (Zhang, Gökce, et al., 2017). During the ablation process, the solution was rotated using a magnetic stirrer (at the revolution of 12 rpm) to achieve a homogenous mixture by avoiding the formation of craters on the target surface.

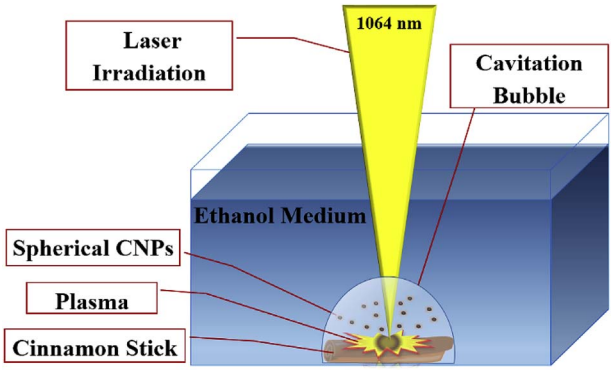

Fig. 1. Schematic diagram of laser ablation development for synthesizing CNPs in ethanol media.

2.3. CNPs characterization

The absorption spectra in the wavelength range of 200–600 nm were recorded on a UV–Vis spectrophotometer (PerkinElmer Lambda 25 Spectrometer). FTIR spectra of the CNPs in the wave number range of 500–4000 cm^{-1} were recorded on a PerkinElmer Frontier™ Spectrometer. The CNPs morphology (size and shape) and selected-area electron diffraction (SAED) pattern was analyzed respectively using a Biological Transmission Electron Microscope (BIO-TEM from Hitachi HT7700) and a High-Resolution Transmission Electron Microscope (HRTEM from JEOL ARM 200F). The samples elemental compositions were detected by Energy Dispersive X-ray (EDX) spectrometer (Field Emission Scanning Electron Microscope, HITACHI SU8020). The Dynamic Light Scattering (DLS) tool was used to measure mean diameter of CNPs. The standard deviation of the CNPs size distribution was determined using the Zetasizer (Nano-ZS90 Malvern Instruments). The chemical degradation of the prepared CNPs was assessed using Liquid Chromatography-Mass Spectrometry (LC-MS operated at 254 nm, Agilent Ion Mobility 6560 Q-TOF system) coupled with the Agilent 1290 Infinity II UHPLC. A reverse-phase C18 column (Poroshell 120 EC-C18, dimension of 4.6 mm × 100 mm × 2.7 μm at 35 °C) was used. In this test, CNPs solution of volume 10 μL was injected into the LC system at the flow rate of 1.0 mL/min. All the characterizations were performed at room temperature.

2.4. Antibacterial activity test of CNPs

Four bacterial cultures were examined using the agar well diffusion method to determine the capacity of CNPs in preventing the bacterial growth. First, the Mueller-Hinton agar was injected into the sterilized Petri dishes and the broth was allowed to solidify. Next, the fresh bacterial cultures (BS, EC, SA, and PA) were swabbed homogeneously over the broth plates using sterile L-shape. Four wells were made (each of diameter 6 mm) on the agar medium plate using sterile cork borer. In each case, about 20 μL of the CNPs solution prepared using different laser ablation energy (30–180 mJ) was poured into the corresponding well. The blank, standard antibacterial agent (penicillin-streptomycin)

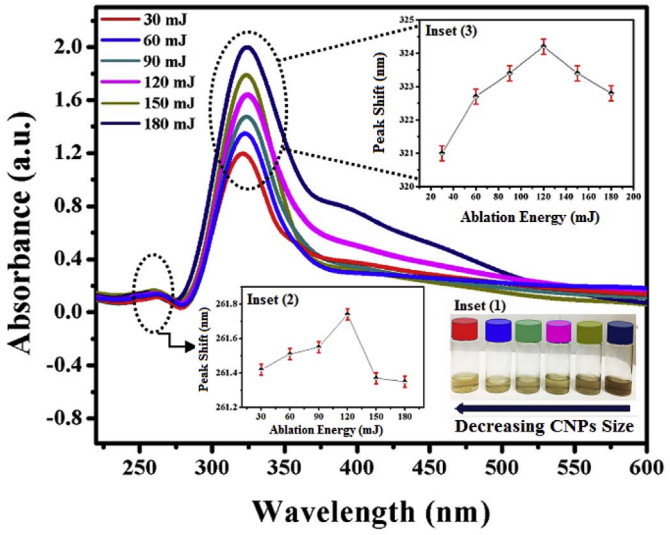

Fig. 2. Optical absorption spectra of CNPs prepared in ethanol medium with different laser ablation energy. Inset (1): CNPs diameter dependent color change, inset (2): peak (minor) shift and inset (3): peak (prominent) shift. (For interpretation of the references to color in this figure legend, the reader is referred to the Web version of this article.)

and the solution without CNPs were utilized to evaluate the antibacterial activity of CNPs. The plates were injected and incubated at 37 °C for 24 h. After the incubation, the appearance of inhibition zone diameter around the injected well was measured to indicate the antibacterial activity of CNPs. The UV–Vis spectrophotometer (PG Instruments, T60 operated at 600 nm) was used to measure the optical density (OD_{600}) of the bacterial growth at each 5 h interval for the total duration of 45 h. Grown bacterial culture of EC, PA, BS and SA each of volume 180 μL (10^4 cells/mL) was incubated. Finally, the CNPs solutions were loaded and added into each flask filled with 20 mL of Muller Hinton broth (at 37 °C) to observe the bacterial cell growth.

3. Results and discussion

Fig. 2 displays the laser ablation energy dependent absorption spectra of the synthesized CNPs. The size, shape and crystallinity of CNPs was altered with the variation of laser ablation energy as evidenced from the change in the absorption peak positions, intensities and solution color. The inset (1) shows that with the increase of laser ablation energy, the colorless solution was gradually turned into dark brown, indicating an increase in the CNPs size. This observation was attributed to the coherent oscillation of electrons at the surface of nanoparticles (Zhang, Gökce, et al., 2017). Furthermore, the absorption intensity (percentage) of the ethanol medium was improved with increasing ablation energy. In short, the NPs size, shape and number density were influenced by the laser ablation energy changes. Two

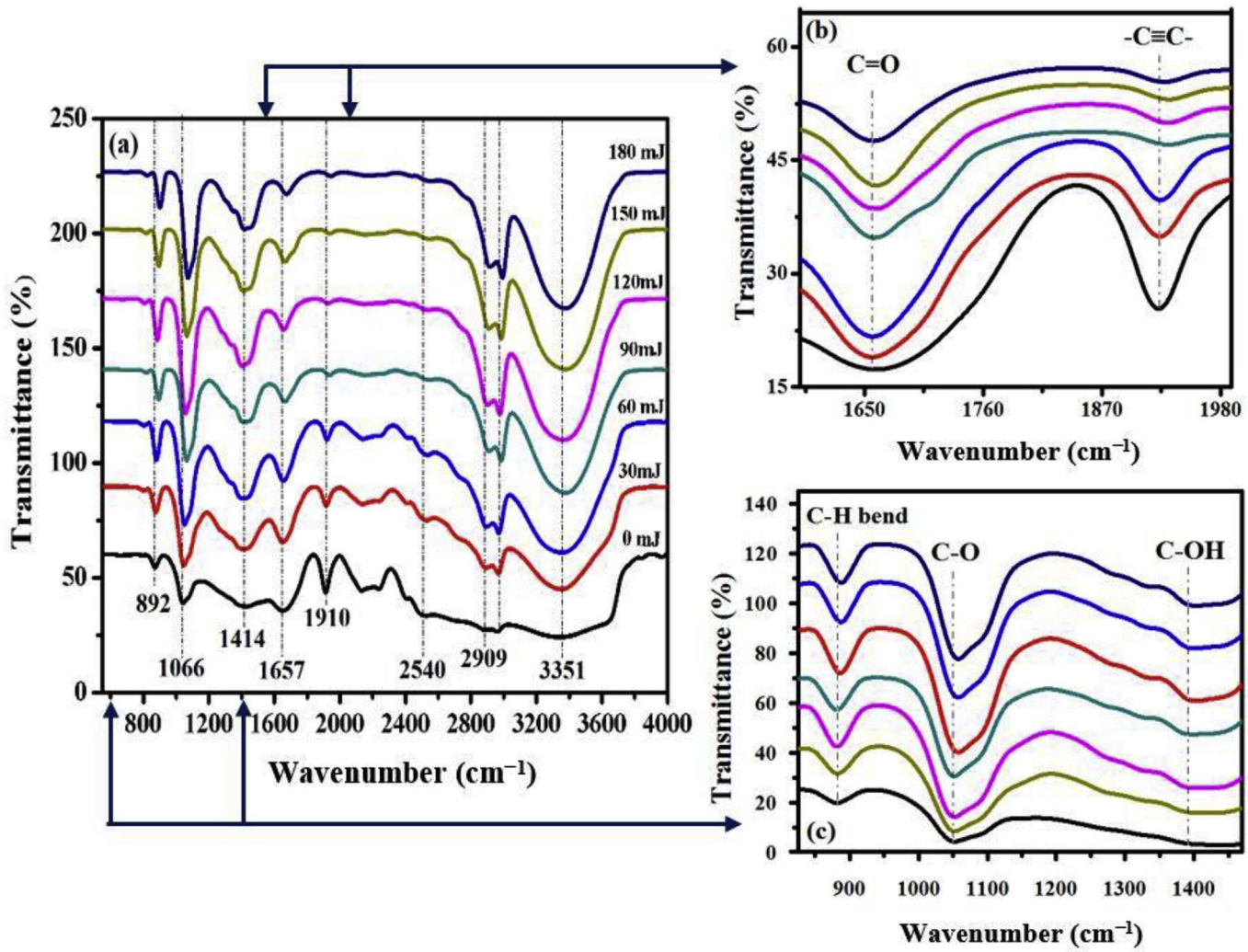

Fig. 3. Laser ablation energy dependent FTIR spectra of CNPs in the wavenumber range of: (a) 500–4000 cm^{-1}, (b) 1600–2000 cm^{-1}, and (c) 800–1500 cm^{-1}.

absorption bands were evidenced around 260 nm and 320 nm, where the bands broadening confirmed the CNPs dispersion in the ethanol medium (Zhang, Gökce, et al., 2017). The prominent absorption band of CNPs was assigned to the presence of phenolic acids in cinnamon and their derivatives (cinnamaldehyde, flavanols and phenylpropenes) as reported (Fatima et al., 2016; Jeyaratnam et al., 2016; Salim & Bidin, 2017). Conversely, the occurrence of the weak peak was allocated to the existence of ring of benzoyl and cinnamoyl system in the nucleated CNPs (Nasrollahzadeh, Sajadi, Babaei, & Maham, 2015; Sharma, 2017). The peak shift toward lower wavelength (Inset (2)) was attributed to the presence of aromatic amino acids and the excitation of tryptophan in the protein (Ahmad et al., 2011). The intensity of the prominent peaks (ranged between 320 and 324 nm) was gradually enhanced accompanied by a red shift (Inset (3)) with the increase of laser ablation energy up to 120 mJ and then blue shifted. This finding was attributed to the quantum size effects of CNPs and consistent with the previous studies (Maruthamuthu & Ramanathan, 2016; Salim et al., 2017). The CNPs liquid suspension was quite stable even over a long time period. This was due to the structural stability of phenols and terpenoids, cinnamaldehyde, carboxyl, eugenol ethyl cinnamate, caryophyllene, existing in the CNPs which contribute to the diverse aroma and biological activities (Ganeev et al., 2004; Jeyaratnam et al., 2016; Salim & Bidin, 2017).

Fig. 3(a) shows the FTIR spectra of all samples which comprised of various functional groups existed in the pure CNPs. The absorption band positions and intensities for CNPs exhibited a minor change. The occurrence of a strong and broad absorption band of CNPs at 3351 cm^{-1} was allocated to the stretching vibration of hydroxyl group (O-H) (Maruthamuthu & Ramanathan, 2016). The absorption band positioned at 2909 and 2540 cm^{-1} was assigned to the carbon hydroxyl (C-H) stretching vibration of alkane (Huang et al., 2007). The absorption band occurred at 1910 cm^{-1} indicated the presence of -C≡C- stretching of alkynes and aldehydes (Maruthamuthu & Ramanathan, 2016). The observed gradual reduction in the absorption intensity of the band around 1910 cm^{-1} (Fig. 3(b)) was ascribed to the formation of CNPs and the oxidation of ethanol (Coronado, Kataoka, Tejedor-Tejedor, & Anderson, 2003). The band located at 1657 cm^{-1} exhibited a nonlinear increase in the intensity with increasing ablation energy, indicating the strong stretching vibration of an aldehyde carbony1 C=O groups of alkenes. These results confirmed the growth of CNPs and supported the observed broadening and shift in UV–Vis absorption bands (Fig. 2). The intense peaks of CNPs (Fig. 3(c)) were allocated to the presence of high amount of aldehydes and cinnamaldehyde in the cinnamon compound as reported (Collins, Markus, Hassett, & Robinson, 2010; Coronado et al., 2003; Maruthamuthu & Ramanathan, 2016; Salim et al., 2017) The absorption band of C-OH alkane (bending vibration) of CNPs was detected at 1414 cm^{-1} (Fig. 3(c)), which indicated the presence of aromatic ring and its conjugation. The peak was broader than that of standard aldehyde compound (Maruthamuthu & Ramanathan, 2016) The band at 1066 cm^{-1} that originated from the C-O stretching of aliphatic amines clearly indicated the consumption of ethanol due to the oxidation. Besides, this band was shifted to higher wavelength accompanied by an increase in the intensity. The band centered at 892 cm^{-1} was also shifted and the intensity was enhanced with the increase of laser ablation energy (Fig. 3(a and c)). This band was originated from the C-H bending vibration of alkyl halides and alkynes, suggesting their participation in the formation of CNPs. Existence of these peaks (Fig. 3(c)) confirmed the covering of CNPs by plant secondary metabolites such as flavonoids, terpenoids, aldehyde, glycosides, phenols, tannins, with functional groups such as ketone, carboxylic acid (Collins et al., 2010). Furthermore, these groups imparted the stability to the CNPs (Table 1).

Fig. 4(a)–(d) show respectively the TEM and HRTEM images, size distribution, crystalline phase, and EDX spectra of CNPs grown at the optimum ablation energy (90 mJ) of ethanol. The morphology of CNPs (Fig. 4(a)) was majorly consisted of spherical shaped nanoparticle of small size. This unique morphology of CNPs revealed by the TEM images was attributed to the generated atoms that were trapped by the existing nuclei during the diffusion-controlled growth process. The inset in Fig. 4(a) depicts the HRTEM image of a single spherical CNP. The corresponding (Fig. 4(a)) CNPs size distribution is shown in Fig. 4(b) where the average size of NP was ≈10.24 nm. Fig. 4(c) illustrates the magnified TEM image of a selected region in (a), where the inset shows the SAED pattern of a single CNP. Varying morphologies of cinnamon nanostructures have also been observed when different laser parameters and liquid media were used (Salim & Bidin, 2017). The edges of the CNP were brighter than the centers, indicating the existence of proteins structure on the surface which supported FTIR results (Salim & Bidin, 2017; Salim et al., 2017). Growth of cinnamon nanocrystallites along different lattice plane with preferred orientation (Inset of Fig. 4(c)) was confirmed by the presence of bright circular spots and concentric rings in the SAED pattern (Salim & Bidin, 2017; Sathishkumar et al., 2009). The presence of different elements in the CNPs prepared at optimum ablation energy of 90 mJ was observed in the EDX spectra (Fig. 4(d)), wherein these peaks indicated the nucleation of CNPs. Detected elements in the CNPs were C, O, K, Ca, Na, Si, Ni, Al, Mo, Fe, B, P, and S. Leading peaks were related to C, O, S, K and Cu elements (table in the Inset of Fig. 4(d)). The presence of S and P peaks were attributed to the protein capping over the CNPs. These findings were supported by the FTIR analysis (Fig. 3). The Cu peak was appeared from the copper grid used to attach the sample.

DLS and LC/MS analysis were performed to determine the effects of laser fluence (ablation energy) on the mean diameter, standard deviation, size distribution, and chemical degradation of the prepared CNPs (Table 2). The mean diameter of CNPs was decreased with the increase of laser fluence due to rupturing and degradation mechanisms (Tsuji et al., 2001; Wagener et al., 2010). The high laser fluence could break off the larger particles (aggregate) to form finer NPs and alter the molecular structures via the oxidation or the disposal of hydrogen into the CNPs samples (Zhang, Gökce, et al., 2017). In the present work, CNPs grown inside ethanol revealed better antibacterial efficacy together with particle size, shape and chemical stability than those produced with other liquid media (Salim & Bidin, 2017; Salim et al., 2017).

Table 1
FTIR band positions and assignments of CNPs compared to the pure bulk cinnamon.

Vibrational band assignments	Wavenumber (cm^{-1})			Vibration modes
	Pure cinnamon	Ethanol medium	CNPs in ethanol with different laser ablation energy	
O-H stretch	3435	3351	3353–3360	Alcohols and Phenols
C-H stretch	2920	2909 and 2540	2911- 2920 and 2544–2553	Alkanes
C≡C stretch	2099	1910	1914–1921	Alkynes and Aldehydes
C=O stretching	1702	1657	1659–1671	Aldehydes and Alkenes
C-OH	1448	1414	1416–1426	Alkanes
C-O stretching	1096	1066	1070–1082	Aliphatic Amines
C-H bending	690	892	895–906	Alkyl Halides

3.1. Mechanism for antibacterial activity of CNPs

Currently, diverse metallic and nonmetallic NPs are regarded as practical alternative to antibiotics due to their great effectiveness towards antibacterial activities. In fact, CNPs reveal physical interaction with the cell walls of various bacteria, which is significant for gram-negative bacteria. Past studies revealed the adhesion and accumulation of diverse NPs to the bacterial walls (Franci et al., 2015). Lately, it has

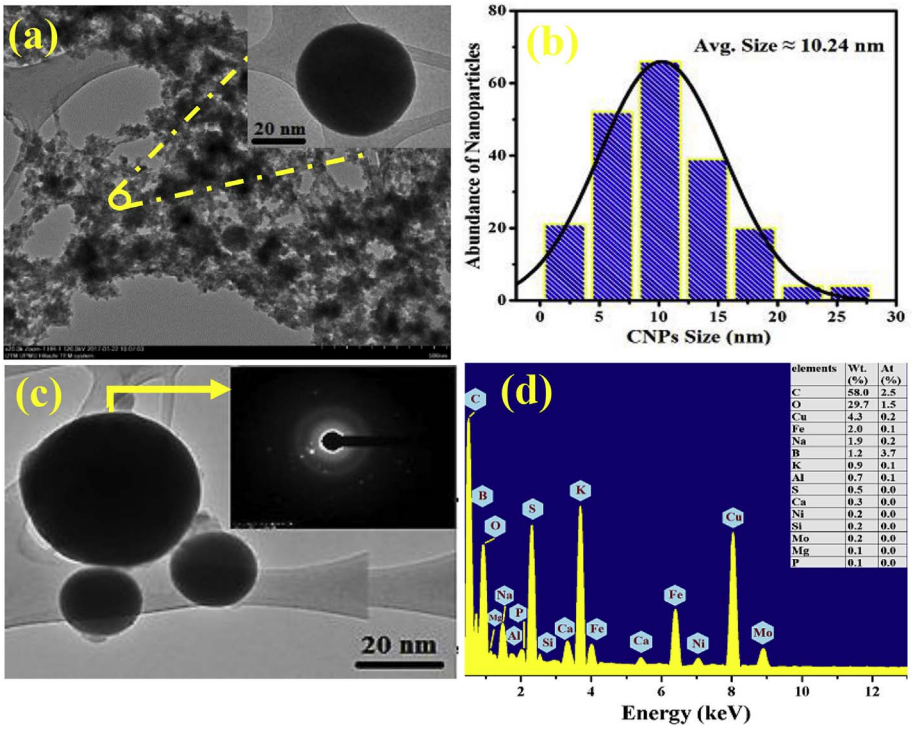

Fig. 4. CNPs synthesized with optimum ablation energy of 90 mJ in ethanol: (a) TEM image of the optimum sample (Inset: HRTEM of single spherical CNP), (b) size distribution of CNPs corresponding to (a), (c) magnified TEM image (Inset: SAED pattern of the marked CNP), and (d) EDX spectra (Inset: Wt.% and At.% of analyzed elements).

Table 2
Laser fluence dependent CNPs mean size (± standard deviation, SD), percentage chemical degradation (Deg) and sample code.

CNPs sample code	Ablation energy (mJ)	Fluence (J/cm^2)	Mean size ± SD (nm)	Deg (%)
S1-30	30	1.91	18.92 ± 1.91	0.08 ± 0.01
S1-60	60	3.82	18.15 ± 3.21	0.25 ± 0.1
S1-90	90	5.73	16.80 ± 0.89	0.4 ± 0.2
S1-120	120	7.64	13.17 ± 0.61	0.7 ± 0.3
S1-150	150	9.55	12.17 ± 0.31	1.1 ± 0.6
S1-180	180	11.46	11.48 ± 0.29	2.7 ± 0.7

been demonstrated that NPs can damage the bacterial cell membranes, leading to structural alteration. Thereby, causing the bacteria to become more permeable (Pal, Tak, & Song, 2007; Salim et al., 2017). It has also been affirmed that the nanoparticles size, shape and concentration play a significant role. Previous researches asserted that the NPs accumulation on the cell membrane can create gaps in the integrity of the bilayer which predisposes to enhance the permeability and eventually bacterial cell death (Franci et al., 2015; Hashimoto et al., 2012). Briefly, it was concluded that NPs antibacterial efficacy is strongly size dependent (Bagherzade, Tavakoli, & Namaei, 2017). Actually, the antibacterial efficacy of small CNPs (< 30 nm) was discerned to be optimal against EC, PA, BS and SA strains (Bagherzade et al., 2017; Salim et al., 2017). The penetration capacity of smaller CNPs into the bacteria is better and their interactions with the membranes, resultant damage, and subsequent cell death are higher than larger one. In this process, a closer interaction occurs between the two entities, promoting possible penetration into the bacterial cell membranes. Indeed, the size distribution of the nanoparticles is a fundamental parameter for controlling the antimicrobial activity.

Nanoparticles with positive charge and reduced size distribution are effective for antibacterial purposes. The surface area to volume ratio of NPs being higher than their bulk counterpart, the modalities and the amount of the interactions with the bacterial surfaces are favored, elevating the antibacterial activities. The cinnamon molecules attaching to the negatively charged protein and nucleic acid can cause structural alteration and distortion in the wall, membranes and nucleic acids of the bacterial cell. The CNPs can also damage the membranes and stimulate the release of reactive oxygen species, forming free radicals with a potent antibacterial action. Furthermore, tiny CNPs can easily penetrate into the microbial body, causing the damage of the intracellular components. Thus, the ribosomes are denatured and protein synthesis is inhibited, preventing the translation and transcription via the bacterial cell binding related genetic material (Bagherzade et al., 2017). It was shown that the protein synthesis can be altered by CNPs treatment. The proteomic results asserted the immature precursors accumulation of membrane proteins, causing a destabilization of the outer membrane composition. Fig. 5 illustrates the probable antibacterial/toxicity mechanisms of CNPs on the bacterial cell (Sharma, 2017).

3.2. Antibacterial properties of CNPs

The antibacterial activity of the prepared CNPs in ethanol medium was carried out using agar well diffusion method. The inhibition zone diameter (1–30 mm) was measured to determine the antibacterial property of the CNPs grown at varying ablation energy. These NPs

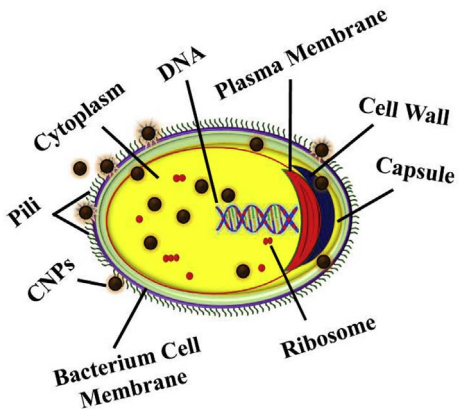

Fig. 5. Schematics showing the activity of CNPs against bacterial strain.

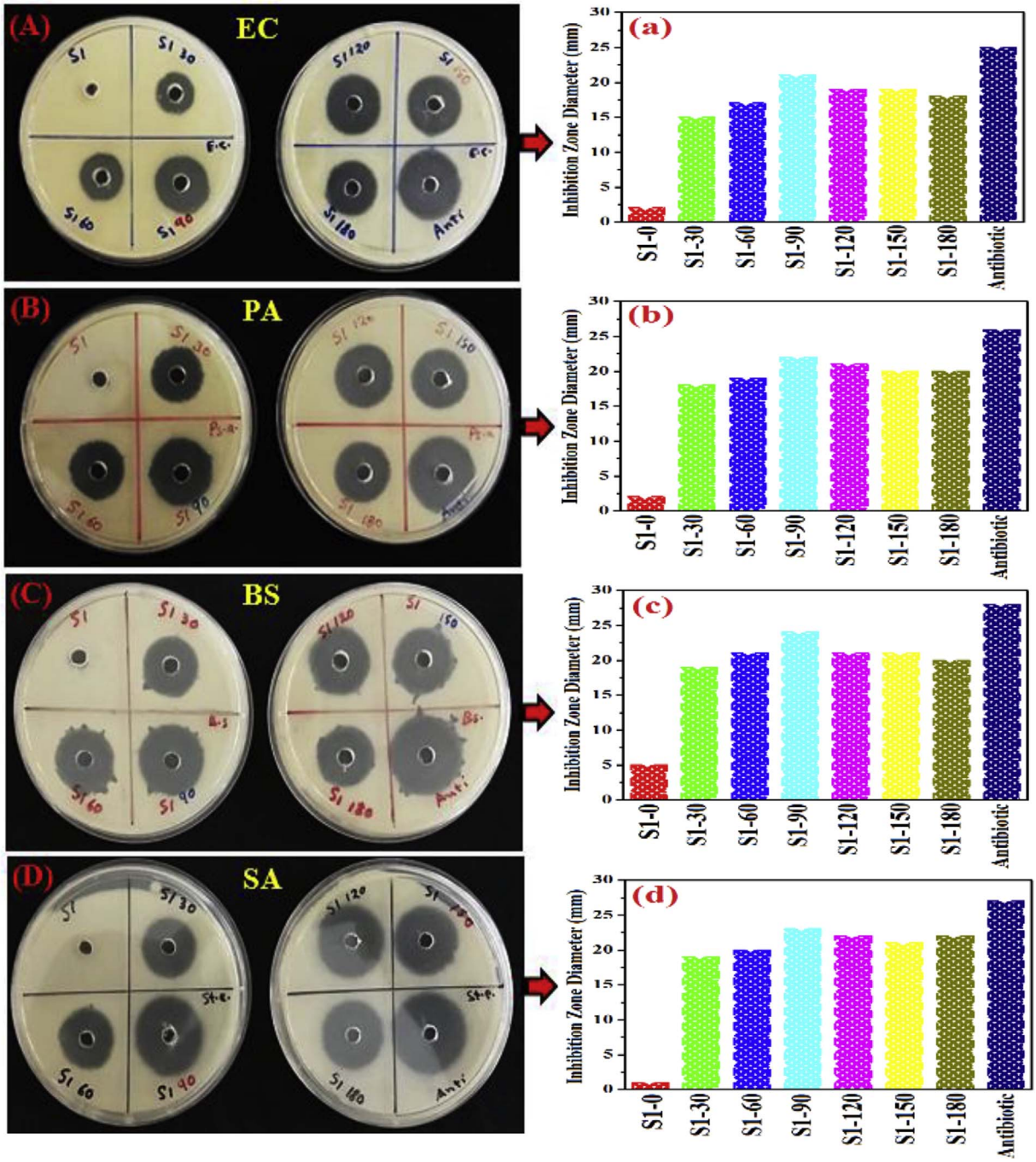

Fig. 6. Inhibition zones diameter revealing the antibacterial activity of CNPs prepared at different laser ablation energy in ethanol medium when applied on bacterial strains of: (A, a) *Escherichia coli*, (B, b) *Pseudomonas aeruginosa*, (C, c) *Bacillus subtilis* and (D, d) *Staphylococcus aureus*.

revealed high inhibitory effect against gram (positive and negative) bacterial strains including EC, PA, BS and SA as displayed in Fig. 6(A–D), respectively. The observation of the largest inhibition zone diameter (in mm) for sample S1-90 grown at optimum ablation energy (90 mJ) verified the strongest antibacterial activity. Likewise, the control sample (S1-0) revealed almost insignificant antibacterial activity. Fig. 6(a–d) respectively illustrates the laser ablation energy dependent inhibition zone diameter for the bacterial strains EC, PA, BS and SA when compared with the antibiotic. The probable mechanism of antibacterial activity of CNPs showed efficient inhibition zone of the bacterial surface protein and subsequent prevention of cell adhesion to fibronectin. It was emphasized that CNPs could anchor to the bacterial cell walls, interrupt the membranes structure, and finally penetrate inside the cells to break down the structure of cell organelles as briefly explained in Section 3.1. It was asserted that the antibacterial activity of CNPs grown inside ethanol media is superior to those produced with methanol (Salim et al., 2017). These observations could be attributed to the high crystallinity, more accurate and narrow size distribution of the CNPs achieved via PLAL technique.

The laser ablation energy dependent optical density of the CNPs measured at 600 nm (OD_{600}) is shown in Fig. 7(a)–(d), where the test was conducted on the bacterial cultures of *Escherichia coli* (*E. coli*), *Staphylococcus aureus* (*S. aureus*), *Bacillus subtilis* (B. subtilis) and *Pseudomonas aeruginosa* (*P. aeruginosa*). The ethanol suspension containing the CNPs was treated in every 5 h interval for the total duration of 45 h to determine the influence of CNPs (grown at different ablation energy)

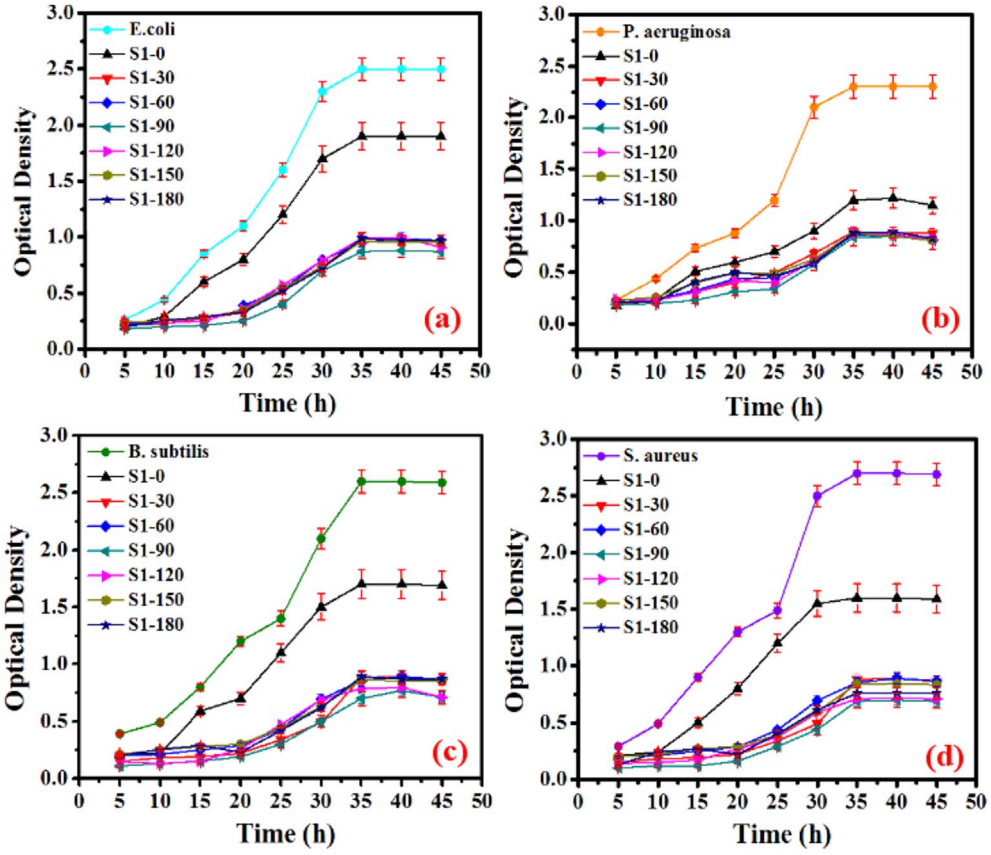

Fig. 7. Optical density (OD_{600}) displaying the bactericidal activity of CNPs prepared at different ablation energy when tested on bacterial strains of: (a) *Escherichia coli*, (b) *Pseudomonas aeruginosa*, (c) *Bacillus subtilis* and (d) *Staphylococcus aureus*.

on the bacterial growth. The achievement of lower OD_{600} for the bacterial suspension after the cultivation for a definite period signified the better antibacterial ability of the reagent (CNPs). The absorption intensity of all the bacterial strains treated without and with CNPs as well as the control sample (S1-0) was depended on the standard inhibition zone (Fig. 6). Additionally, in each 5 h of cultivation, the broth samples of the bacterial strains containing CNPs revealed lower OD_{600}, which was attributed to the reduction of CNPs conglomeration. The suspension containing optimum CNPs (S1-90) exhibited the lowest OD_{600} after 10 h of cultivation, where the effect of average diameter was the lowest (16.80 nm). This observation was attributed to the large surface area to volume ratio of the CNPs that played a significant role on the bacterial strains growth. It was concluded that CNPs possess a superior capacity to resist the growth of bacteria. In fact, these CNPs (grown inside the ethanol media) with highly spherical morphologies could delay the bacterial growth more efficiently than those produced inside methanol (Salim et al., 2017). Thus, it was established that ethanol as growth media for the production of CNPs using PLAL technique is certainly better than methanol (Salim et al., 2017).

4. Conclusion

For the first time, the antibacterial effectiveness of spherical CNPs grown in ethanol using PLAL technique was evaluated. Highly crystalline, natural and spherical CNPs were achieved by varying the laser ablation energy. These NPs were demonstrated to be effective for antibacterial purposes. The structure, morphology, optical properties and antibacterial activity of such CNPs were found to be sensitive to the variation of laser ablation energy. Systematic characterizations of the prepared CNPs (at room temperature) revealed the feasibility of controlling their morphology (shape and size) in a desirable manner which is advantageous for medicinal applications. In addition, present technique can produce high yields and easy to operate in the absence of any toxic reagents or surfactant template. UV–Vis spectra revealed two characteristic bands in the range of 260 and 320 nm. The optimum CNPs (grown at 90 mJ) exhibited highest antibacterial activity. The agar dilution and diffusion test were conducted to evaluate the antibacterial activity of the as-synthesized CNPs against EC, PA, BS and SA bacterial strains. The observed strong antibacterial activity of the CNPs was ascribed to their quantum size effect and unique morphology. It was affirmed that ethanol as growth media for CNPs could be better than the other reported media involving the morphologies and antibacterial activities. It was also established that the proposed natural CNPs with intrinsic antibacterial efficacy may be greatly beneficial for the development of nanobiomedicine.

Acknowledgments

Authors are thankful to Malaysian Ministry of Education for the financial assistance through Vot. FRGS 4F815 and GUP/RU 17H19/13H50.

References

Ahmad, N., Sharma, S., Alam, M. K., Singh, V. N., Shamsi, S. F., Mehta, B. R., et al. (2010). Rapid synthesis of silver nanoparticles using dried medicinal plant of basil. *Colloids and Surfaces B: Biointerfaces, 81*, 81–86.

Ahmad, N., Sharma, S., Alam, M. K., Singh, V. N., Shamsi, S. F., Mehta, B. R., et al. (2011). Biosynthesis of silver nanoparticles from desmodium triflorum: A novel approach towards weed utilization. *Biotechnology Research International, 2011*, 8.

An, B. K., Kwon, S. K., Jung, S. D., & Park, S. Y. (2002). Enhanced emission and its switching in fluorescent organic nanoparticles. *Journal of the American Chemical Society, 124*, 14410–14415.

Asahi, T., Sugiyama, T., & Masuhara, H. (2008). Laser fabrication and spectroscopy of organic nanoparticles. *Accounts of Chemical Research, 41*, 1790–1798.

Bagherzade, G., Tavakoli, M. M., & Namaei, M. H. (2017). Green synthesis of silver nanoparticles using aqueous extract of saffron (Crocus sativus L.) wastages and its antibacterial activity against six bacteria. *Asian Pacific Journal of Tropical Biomedicine, 7*, 227–233.

Basniwal, R. K., Buttar, H. S., Jain, V. K., & Jain, N. (2011). Curcumin nanoparticles:

Preparation, characterization and antimicrobial study. *Journal of Agricultural and Food Chemistry, 59*, 2056–2061.
Chang, S. T., Chen, P. F., & Chang, S. C. (2001). Antibacterial activity of leaf essential oils and their constituents from cinnamomum osmophloeum. *Journal of Ethnopharmacology, 77*, 123–127.
Collins, T. L., Markus, E. A., Hassett, D. J., & Robinson, J. B. (2010). The effect of a cationic porphyrin on pseudomonas aeruginosa biofilms. *Current Microbiology, 61*, 411–416.
Coronado, J. M., Kataoka, S., Tejedor-Tejedor, I., & Anderson, M. A. (2003). Dynamic phenomena during the photocatalytic oxidation of ethanol and acetone over nanocrystalline TiO2: Simultaneous FTIR analysis of gas and surface species. *Journal of Catalysis, 219*, 219–230.
Fatima, M., Zaidi, N. U., Amraiz, D., & Afzal, F. (2016). In vitro antiviral activity of cinnamomum cassia and its nanoparticles against H7N3 influenza a virus. *Journal of Microbiology and Biotechnology, 26*, 151–159.
Franci, G., Falanga, A., Galdiero, S., Palomba, L., Rai, M., Morelli, G., et al. (2015). Silver nanoparticles as potential antibacterial agents. *Molecules, 20*, 8856–8874.
Ganeev, R., Baba, M., Ryasnyansky, A. I., Suzuki, M., & Kuroda, H. (2004). Characterization of optical and nonlinear optical properties of silver nanoparticles prepared by laser ablation in various liquids. *Optics Communications, 240*, 437–448.
Gopinath, V., MubarakAli, D., Priyadarshini, S., Priyadharsshini, N. M., Thajuddin, N., & Velusamy, P. (2012). Biosynthesis of silver nanoparticles from tribulus terrestris and its antimicrobial activity: A novel biological approach. *Colloids and Surfaces B: Biointerfaces, 96*, 69–74.
Hashimoto, M. C., Prates, R. A., Kato, I. T., Nunez, S. C., Courrol, L. C., & Ribeiro, M. S. (2012). Antimicrobial photodynamic therapy on drug-resistant pseudomonas aeruginosa-induced infection: An in vivo study. *Photochemistry and Photobiology, 88*, 590–595.
Huang, J., Li, Q., Sun, D., Lu, Y., Su, Y., Yang, X., et al. (2007). Biosynthesis of silver and gold nanoparticles by novel sundried cinnamomum camphora leaf. *Nanotechnology, 18* 105–104.
Jeyaratnam, N., Nour, A. H., Kanthasamy, R., Nour, A. H., Yuvaraj, A. R., & Akindoyo, J. O. (2016). Essential oil from cinnamomum cassia bark through hydrodistillation and advanced microwave assisted hydrodistillation. *Industrial Crops and Products, 92*, 57–66.
Ma, Q., Davidson, P. M., Critzer, F., & Zhong, Q. (2016). Antimicrobial activities of lauric arginate and cinnamon oil combination against foodborne pathogens: Improvement by ethylenediaminetetraacetate and possible mechanisms. *LWT-Food Science and Technology, 72*, 9–18.
Maruthamuthu, R., & Ramanathan, K. (2016). Phytochemical analysis of bark extract of cinnamomum verum: A medicinal herb used for the treatment of coronary heart disease in Malayali tribes. *International Journal of Pharmacognosy and Phytochemical Research, 8*, 1218–1222.
Müller, R. H., Jacobs, C., & Kayser, O. (2001). Nanosuspensions as particulate drug formulations in therapy: Rationale for development and what we can expect for the future. *Advanced Drug Delivery Reviews, 47*, 3–19.
Nasrollahzadeh, M., Sajadi, S. M., Babaei, F., & Maham, M. (2015). Euphorbia helioscopia linn as a green source for synthesis of silver nanoparticles and their optical and catalytic properties. *Journal of Colloid and Interface Science, 450*, 374–380.
Pal, S., Tak, Y. K., & Song, J. M. (2007). Does the antibacterial activity of silver nanoparticles depend on the shape of the nanoparticle, A study of the gram-negative bacterium Escherichia coli. *Applied and Environmental Microbiology, 73*, 1712–1720.
Sajti, C. L., Sattari, R., Chichkov, B. N., & Barcikowski, S. (2010). Gram scale synthesis of pure ceramic nanoparticles by laser ablation in liquid. *The Journal of Physical Chemistry C, 114*, 2421–2427.
Salim, A. A., & Bidin, N. (2017). Pulse Q-switched Nd: YAG laser ablation grown cinnamon nanomorphologies: Influence of different liquid medium. *Journal of Molecular Structure, 1149*, 694–700.
Salim, A. A., Bidin, N., Lafi, A. S., & Huyop, F. Z. (2017). Antibacterial activity of PLAL synthesized nanocinnamon. *Materials and Design, 132*, 486–495.
Sathishkumar, M., Sneha, K., Won, S. W., Cho, C. W., Kim, S., & Yun, Y. S. (2009). Cinnamon zeylanicum bark extract and powder mediated green synthesis of nanocrystalline silver particles and its bactericidal activity. *Colloids and Surfaces B: Biointerfaces, 73*, 332–338.
Sharma, S. (2017). Enhanced antibacterial efficacy of silver nanoparticles immobilized in a chitosan nanocarrier. *International Journal of Biological Macromolecules, 104*, 1740–1745.
Sylvestre, J. P., Kabashin, A. V., Sacher, E., Meunier, M., & Luong, J. H. (2004). Stabilization and size control of gold nanoparticles during laser ablation in aqueous cyclodextrins. *Journal of the American Chemical Society, 126*, 7176–7177.
Tsuji, T., Iryo, K., Nishimura, Y., & Tsuji, M. (2001). Preparation of metal colloids by a laser ablation technique in solution: Influence of laser wavelength on the ablation efficiency (II). *Journal of Photochemistry and Photobiology A: Chemistry, 145*, 201–207.
Wagener, P., Schwenke, A., Chichkov, B. N., & Barcikowski, S. (2010). Pulsed laser ablation of zinc in tetrahydrofuran: Bypassing the cavitation bubble. *The Journal of Physical Chemistry C, 114*, 7618–7625.
Yang, X., Yang, X., Li, Q., Wang, H., Huang, J., Lin, L., et al. (2010). Green synthesis of palladium nanoparticles using broth of cinnamomum camphora leaf. *Journal of Nanoparticle Research, 12*, 1589–1598.
Yildirim, S. T., Oztop, M. H., & Soyer, Y. (2017). Cinnamon oil nanoemulsions by spontaneous emulsification: Formulation, characterization and antimicrobial activity. *LWT-Food Science and Technology, 84*, 122–128.
Zhang, D., Gökce, B., & Barcikowski, S. (2017a). Laser synthesis and processing of colloids: Fundamentals and applications. *Chemical Reviews, 117*, 3990–4103.
Zhang, S., Zhang, M., Fang, Z., & Liu, Y. (2017b). Preparation and characterization of blended cloves/cinnamon essential oil nanoemulsions. *LWT-Food Science and Technology, 75*, 316–322.